The regulatory landscape of *Arabidopsis thaliana* roots at single-cell resolution

Authors: Michael W. Dorrity[1], Cris Alexandre[1], Morgan Hamm[1], Anna-Lena Vigil[3], Stanley Fields[1,2], Christine Queitsch[1] and Josh Cuperus[1]

Affiliations:
[1] Department of Genome Sciences, University of Washington, Seattle, WA 98195
[2] Department of Medicine, University of Washington, Seattle, WA 98195
[3] School of Life Sciences, University of Nevada, Las Vegas, NV 89154

[†] Correspondence to Christine Queitsch (queitsch@uw.edu) and Josh Cuperus (cuperusj@uw.edu)

Abstract: In plants, chromatin accessibility – the primary mark of regulatory DNA – is relatively static across tissues and conditions. This scarcity of accessible sites that are dynamic or tissue-specific may be due in part to tissue heterogeneity in previous bulk studies. To assess the effects of tissue heterogeneity, we apply single-cell ATAC-seq to A. thaliana roots and identify thousands of differentially accessible sites, sufficient to resolve all major cell types of the root. However, even this vast increase relative to bulk studies in the number of dynamic sites does not resolve the poor correlation at individual loci between accessibility and expression. Instead, we find that the entirety of a cell's regulatory landscape and its transcriptome each capture cell type identity independently. We leverage this shared information on cell identity to integrate accessibility and transcriptome data in order to characterize developmental progression, endoreduplication and cell division in the root. We further use the combined data to characterize cell type-specific motif enrichments of large transcription factor families and to link the expression of individual family members to changing accessibility at specific loci, taking the first steps toward resolving the direct and indirect effects that shape gene expression. Our approach provides an analytical framework to infer the gene regulatory networks that execute plant development.

Introduction

Single-cell genomics allows an unbiased sampling of cells during development, with the potential to reveal the order and timing of gene regulatory and gene expression events that specify cell identity and lineage. An ideal system to test the ability of single-cell genomics to provide novel insights into development is the *Arabidopsis thaliana* root: along its longitudinal axis, a single, radially-symmetric root captures developmental trajectories for several radially-symmetric cell types. Approaches in this organism have included single-cell RNA-seq to transcriptionally profile individual root cell types along this developmental axis[1–6] and with respect to their ploidy.

Studies of chromatin accessibility in samples enriched for specific plant cell types have revealed: (i) the existence of cell type-specific regulatory elements; (ii) the relative scarcity of such elements compared to their prevalence in animals or humans; (iii) the expected enrichment of transcription factor binding sites within these elements; and (iv) a higher frequency of dynamic regulatory elements upstream of environmentally-responsive genes than constitutively expressed genes.[7,8] Although the correlation between chromatin accessibility and nearby gene expression is generally weak in both plants and animals,[9] this correlation improves for regulatory elements that show dynamic changes in chromatin accessibility, for example in response to an environmental stimulus or developmental signal.[7,9–11] In contrast to animals, however, the majority of chromatin-accessible sites in plants show little change across tissues, conditions, or even genetic backgrounds, raising the possibility that cell and tissue identity is less rigidly engrained in the chromatin landscape in plants than in animals.[7] Alternatively, cell type-specific regulatory elements and gene expression in plants may have been obscured by tissue heterogeneity in bulk tissue studies.

Cell type-specific chromatin-accessible landscapes are also of interest for addressing other fundamental biological questions. General transcription decreases along a cell type's developmental trajectory while expression of cell type-specific genes increases,[2,12,13] in agreement with Waddington's predictions on epigenetic landscapes.[14] In the *A. thaliana* root, the increasing maturity of certain cell layers is accompanied by endoreduplication. The presence of additional gene copies may contribute to the observed increase in the expression of cell type-specific genes; alternatively, the initial gene copies may increase their transcription. Although endoreduplication is a common mechanism to regulate cell size and differentiation in plants and some human and animal tissues,[15–17] the influence of this phenomenon on gene regulation and expression has been largely overlooked. In plants, endoreduplication generally enhances transcription,[17,18] in particular of cell-wall-related genes[19] and genes encoding ribosomal RNA,[20] hinting at a role for this process in driving increased translation.

Here, we provide the first single-cell resolution maps of open chromatin in the *A. thaliana* root to address the issue of tissue heterogeneity and to detect likely endoreduplication events. We use a droplet-based approach to profile over 5000 nuclei for chromatin accessibility and identify 8000 regulatory elements that together define most cell types of the root. We describe an analytical framework that links patterns of open chromatin with transcriptional states to predict the identity, function and developmental stage of individual cells in the *A. thaliana* root. We integrate the single-cell ATAC-seq (scATAC-seq) data with published single-cell RNA-seq (scRNA-seq) profiles of the same tissue to obtain automated cell annotations of scATAC cells. Using the integrated dataset, we link individual scATAC cells with their nearest neighbors in scRNA space to define relative developmental progression, level of endoreduplication and the genes differentially expressed in these nearest neighbors. This approach allows the identification of three distinct developmental states of endodermis cells that

had escaped detection using scRNA-seq alone. Using integrated scRNA-seq data, we predict individual members of large transcription factor families that play a role in epidermis development, pinpointing individual regulatory events that link peak accessibility and transcription factor expression in these cells. The combination of binding motifs, transcription factor expression and chromatin accessibility provides a basis for predicting the gene regulatory events that underlie development.

Results

scATAC-seq identifies known root cell types

We first asked if ATAC-seq profiles at the single-cell level were capable of capturing known root cell types. We profiled 5283 root nuclei, at a median of 7290 unique ATAC inserts per cell. A high fraction of these inserts occurred in one of the 21,889 open chromatin peaks (FRIP score = 0.71) based on pseudo-bulk peak calling (Cellranger v3.1, 10X Genomics); this fraction is similar to that seen in high-quality bulk accessibility studies (**Figure S1A, S1B**).[9] We used UMAP dimensionality reduction of the peak by cell matrix to build a two-dimensional representation grouping of cells with similar accessibility profiles (**Figure 1A**). Subsequent cluster assignment by Louvain community detection identified nine distinct cell clusters.[21] Across all cell types, we identified 7910 peaks (ranging from 939 – 2065 per cell type) with significant differential accessibility, suggesting that around a third of all accessible sites contain some information on cell type (**Supplementary Table 1**). To assign cell type annotations to each of these clusters, we generated "gene activity" scores that sum all ATAC inserts within each gene body and 400 bp upstream of its transcription start site. This approach rests on the assumption that a chromatin-accessible site in the compact *A. thaliana* genome tends to be associated with regulation of its most proximal gene.[22] While this assumption may not hold universally, gene activity scores offer the advantage of allowing a direct comparison to bulk ATAC-seq and single-cell RNA-seq datasets through a matched feature set. In this way, we identified genes whose accessibility signal specifically marks each cell cluster. We visualized peaks with cell type-specific accessibility by grouping cells of a similar type and "pseudobulking" their insert counts at each position in the genome (**Figure 1B**). Cell type-specific ATAC tracks that resemble those obtained in prior whole tissue and cell type enrichment-based ATAC-seq studies for the root (**Figure 1B**).[11]

We used comparisons to tissue-specific genes that were identified from single-cell RNA-seq studies of the *A. thaliana* root to assign a cell type to each cluster defined by ATAC markers from "gene activity" scores.[2,5,6] We identified 210 genes with unique accessibility patterns across all cell types (**Supplementary Table 2**); FRIP scores, fragment lengths, and total read counts did not vary greatly across cell types (**Figure S1C, S1D, S1E**). For each cell type, the median number of genes with tissue-specific accessibility was 20 (range 5 to 53) (**Figure 1C**). This small number of genes is

consistent with earlier studies that show few open chromatin sites that define cell type identity in *A. thaliana*.[7,23] Although thousands of differentially accessible sites have been found across tissue types,[7] accessibility differences between more closely related cell types remains largely unexplored, with the exception of root hair vs non-hair, in which very few differences were found.[7,11] For three cell clusters (959 cells, or 18% of cells), we could not identify a coherent set of a markers and therefore could not annotate them (grey points, **Figure 1A**). However, all other cell clusters were manually annotated and corresponded to the major cell layers of the root: outer layers including epidermis cortex, and a precursor of endodermis and cortex (ec pre); endodermal layers comprised of three distinct types (endo 1, 2, and 3); and the stele comprised of two main types along with a phloem type (stele phloem). In general, ATAC marker genes did not show a strong overlap with RNA-based marker genes. Endodermis cells were an exception, as several of their ATAC marker genes (AT3G32980, AT1G61590, AT1G14580, AT3G22600, AT5G66390) were also found to be marker genes in single-cell RNA-seq studies.[24] While this lack of overlap makes annotation more challenging, it is consistent with the reported weak correlation of chromatin accessibility with gene expression.[23,25] Moreover, the finding that expression levels are not precisely predicted by nearby accessible sites suggests that accessibility can add orthogonal information about cell identity to further stratify cell types into distinct subtypes.

Sequences motifs of transcription factor families associate with cell type-specific sites of open chromatin

Accessibility at regulatory sites is driven by transcription factor binding and modification of local chromatin.[26] We examined if any of the cell type-specific accessible sites were associated with the presence of transcription factor binding motifs. To do so, we used a set of representative motifs for all *A. thaliana* transcription factor families and nearly every individual transcription factor[27] to tally these motif counts within all 21,889 peaks in the full scATAC-seq dataset to build a peak-by-motif matrix. As each peak can be described in terms of its relative accessibility in each of the identified cell types, we performed a linear regression for each motif to test for significant association of accessibility and motif presence. Relative accessibility values were calculated by first pseudo-bulking all peak counts by cell type and then normalizing these cell type-specific peak accessibility scores to a background peak accessibility of all cells pooled together. By testing the association of motif counts and cell type-specific accessibility, we identify transcription factor binding motifs whose presence is correlated with more accessibility in each cell type.

We found significant associations with motifs from at least one transcription factor family in all cell types (**Figure 1D**). For example, relative chromatin accessibility in epidermal cells was strongly associated (q-values ranging from 1e-24 to 1e-133) with the presence of motifs from the WRKY transcription factor family; this family includes *TTG2*, which, along with *TTG1* and *GL2*, has important roles in atrichoblast

173 fate in the epidermis.[28] Furthermore, the effects of each motif family on relative
174 accessibility was sufficient to hierarchically cluster cell types according to broad tissue
175 classes (**Figure 1D**). Based on similarities in motif associations, hierarchical clustering
176 grouped all stele clusters (1, 2, and 11), epidermis and cortex (clusters 0 and 3), two
177 endodermis clusters (4 and 10), and another endodermis cluster with epidermal
178 precursor cells (clusters 7 and 8). That motif associations alone can distinguish among
179 clusters and group similar ones together provides independent verification of the cell
180 type-specific nature of the chromatin-accessible sites detected in the scATAC-seq
181 data.
182
183 **Epidermal cell layers show increased levels of endoreduplication**
184
185 In contrast to scRNA-seq data, scATAC-seq data can provide insight into DNA
186 copy number and its impact on gene regulation. DNA copy number is of special
187 relevance in the *A. thaliana* root, as each cell layer undergoes different rates of
188 endoreduplication.[19] In a diploid cell, a single accessible locus tends to show 1 or 2
189 transposition events. In polyploid cells with higher DNA copy number, a single
190 accessible locus could show 4, 8, or even 16 transpositions. Therefore, cells containing
191 a large number of peaks with >1 transposition event are likely to represent
192 endoreduplicated cells. To identify such cells, we classified each cell by the mean
193 number of cuts it contained per peak and examined the distribution of this metric to
194 draw a threshold above which cells were classified as likely endoreduplicated (**Figure**
195 **S5A, S5B**). We examined the fraction of likely endoreduplicated cells per cell type and
196 compared these fractions to orthogonal measurements of endoreduplication. We found
197 the expected trend of higher endoreduplication in the outermost cell files, with reduced
198 prevalence in the stele (**Figure S5C**). Endoreduplicated cells also showed less total
199 complexity in accessible genes, consistent with their increased developmental
200 progression (**Figure S3G, S3H**).[2]
201
202
203 **Integration of scATAC and scRNA-seq data improves cell type annotation**
204
205 Because scATAC-seq data both identified known root cell types and provided
206 novel cell identity assignments not identifiable through scRNA-seq, we addressed
207 whether combining these two data sets results in additional insights than what could
208 be gained from either alone. We first addressed whether both data types could be
209 embedded in the same low-dimensional space in a manner that maintains the cell
210 identities defined by both scATAC-seq and scRNA-seq. Such embedding assumes
211 that the underlying cell identities represented in each dataset are similar. In this case,
212 the root tissue sampled for the scATAC-seq experiment and previous scRNA-seq
213 experiments was similar and therefore should represent similar numbers and types of
214 cells. Moreover, the data generated by both methods share “gene” as a feature, *i.e.*
215 accessibility near or within a given gene; expression of a given gene.

We used the anchor-based multimodal graph alignment tool from the Seurat package to find nearest-neighbor scRNA-seq matches for each cell in the scATAC-seq data.[29,30] In short, the tool identifies representative features (shared "anchor" genes in our case) in each dataset and looks for underlying correlation structure of those features to group similar cells in a co-embedded space. We plotted all cells within the resulting co-embedded space with cell type labels from each dataset separately. Cells derived from scRNA-seq and scATAC-seq experiments were well mixed (**Figure 2A**). Moreover, we found that cells of the same type were co-localized independent of the source data (**Figure 2B, 2C**), though some separation by data type was apparent, likely owing to the imputation step of dataset integration.[29] This result suggests that RNA and ATAC signals, which are only poorly correlated in bulk studies, are capable of grouping cell identities when determined in individual cells of a complex tissue. We further used this co-embedded space to refine our earlier manual cell type annotations by transferring labels of neighboring scRNA cells onto the scATAC cells (**Figure S2B**); while most of these labels matched, the greatest number of mismatches was seen in endodermis sub-type 3. The transferred labels matched our manual annotations, and, in the case of epidermal cells, allowed us to separate a single ATAC cluster into hair and non-hair cells (**Figure 2A, Figure S2A**). The three distinct ATAC clusters that were assigned an "endodermis" label with this approach are a striking example of scATAC data yielding greater stratification of cell types than the generally richer scRNA data.

scATAC-seq captures three distinct endodermis types representing different developmental stages

We dissected the three endodermis clusters in greater detail using three approaches: (i) by identifying differentially accessible sites among subtypes; (ii) by aligning these subtypes to scRNA-seq data that have been annotated for endoreduplication and developmental progression; and (iii) by determining differentially expressed genes in the nearest-neighbors to each of these endodermis subtypes in scRNA-seq space (**Figure 3A**).

We identified few differentially accessible peaks genes (adjusted p-value < 0.05 and at least 2-fold change in accessibility) in each endodermis subtype: 25 for the first subtype, 24 for the second, and 17 for the third (**Figure 3A**). The low number of associated genes precluded gene set enrichment analyses, but genes uniquely accessible in subtype 1 included transcription factors *NAC010* (AT1G28470) and *MYB85* (AT4G22680) as well as genes involved in suberization (*FAR1*, *FAR4*, *FAR5*). Endodermis subtype 2 showed increased accessibility at *ANAC038* (AT2G24430), *HIPP04* (AT1G2900), encoding a heavy metal-associated protein, and phenylpropanoid metabolism genes. Endodermis subtype 3 showed strong accessibility at the *BLUEJAY* (AT1G14580) locus encoding a C2H2 transcription factor implicated in endodermis differentiation (**Figure 3B, S6A**), as well as at genes for phenylpropanoid biosynthesis.

We addressed whether these differentially-accessible genes show different expression patterns in endodermis cells in scRNA-seq space by mapping expression of each gene onto a subclustered set of endodermis cells combined from several scRNA-seq studies of the *A. thaliana* root. The small set of marker genes for each scATAC subtype showed no consistent pattern in the scRNA-seq data (**Figure S3C**), suggesting that some other feature distinguished these three subtypes.

Structure within two-dimensional embeddings of scRNA-seq and scATAC-seq data derived from developing tissues is often associated with developmental progression or other asynchronous processes like the cell cycle. Furthermore, root tissue has the unique feature of being highly endoreduplicated, which could also account for differences among the subtypes. To assess whether the endodermal subtypes were associated with these features, we added annotations for cell cycle, developmental progression and endoreduplication to the combined root scRNA-seq data and used data integration (as in **Figure 2**) to test whether cells from the endodermal subtypes were associated with any of these features (**Figure S2C**).

We used a list of known cell-cycle marker genes to generate a signature score marking proliferating cells (Arabidopsis.org). This signature score identified cycling cells in other cell types, such as early epidermis cells near the quiescent center (**Figure S4A, S4B**), but showed no difference in the nearest-neighbor cells corresponding to each epidermis subtype (**Figure S4C**). We conclude that cell cycle does not distinguish the epidermis subtypes.

We assessed developmental progression with two orthogonal methods: (i) correlation with published bulk expression data taken along longitudinal sections of the root;[1] and (ii) a modified measure of loss in transcriptional diversity (see Methods), which correlates strongly with developmental progression in a large number of scRNA-seq datasets, including of the *Arabidopsis* root.[2,31] We found that the developmental progression metric as measured by loss in transcriptional diversity was strongly associated with the orthogonal correlation-based classification (**Figure S3A**).[31] For each cell of the endodermal subtypes, we calculated the average developmental progression of its 25 nearest neighbors among root scRNA-seq cells (**Figure S3H, S3J**) and found, assigning this average to each ATAC endodermis cell, a trend of developmental progression among the endodermis sub-types (**Figure 3C**). This result was robust to changes in the number of neighbors used to identify similar cells from scRNA-seq data (**Figure S3D**). This trend was the same if we calculated the developmental progression metric based on scATAC-seq data alone (**Figure S3F**).[31] Cells from subtype 1 were the least developed, while cells from subtype 3 tended to co-occur with the most mature endodermal cells in the co-embedded graph (**Figure 3C**). We conclude that the three endodermal subtypes primarily represent cells of differing developmental progression and that differences in chromatin accessibility are able to capture this stratification of endodermis maturity.

302
303 Developmental progression in the root is often associated with increased ploidy
304 through endoreduplication. To identify endoreduplicated cells in scRNA-seq data, we
305 used a published set of marker genes for ploidy to generate signature scores for 2n,
306 4n, 8n and 16n ploidies.[19] With these scores, we predicted endoreduplicated cells by
307 calculating, for each cell, the ratio of the 8n signature relative to the diploid signature.
308 Similar to the DNA-based metric, this transcriptional approach identified
309 endoreduplicated root cells in the expected pattern (**Figure S3B, S3E**), with higher
310 fractions in the epidermis cell layer and diminished levels in the stele (**Figure S5D**).
311 Because the DNA-based metric showed poorer correlation to prior data and was less
312 sensitive (**Figure S3F, S3G**), we used the transcriptionally-based metric in subsequent
313 analyses. This metric captured an abundance of tetraploid xylem cells in the stele
314 (**Figure S5E**), consistent with previous findings.[19] With confidence in this classifier of
315 endoreduplicated cells, we examined the predicted ploidy for the nearest RNA-seq
316 neighbors of each endodermis subtype (**Figure S3I**). We found that the younger
317 endodermis subtype 1 cells had mostly 2n neighbor cells, while the more mature
318 subtypes 2 and 3 had mostly endoreduplicated neighbor cells, with similar levels in
319 each (**Figure 3D**).
320
321 To better understand the differing transcriptional and chromatin accessibility
322 patterns among endodermis subtypes, we predicted differentially expressed genes
323 for each endodermis subtype (**Figure S2B**). The early endodermis type, which is not yet
324 endoreduplicated showed an enrichment of genes (**Supplementary Table 3**) involved
325 in Casparian strip formation (*CASP3*, *CASP5*) and wax biosynthesis (HHT1). The
326 intermediate subtype 2 also showed enrichment for genes involved in Casparian strip
327 formation (*CASP3*, *CASP4*, *CASP5*, *GSO1*), as well as mechanosensitive ion channels
328 (*MSL4*, *MSL6*, *MSL10*) (**Supplementary Table 4**). The most advanced endodermis
329 subtype 3 showed enrichment for stress responses and metabolism of toxic
330 compounds, kinase activity, and high levels of aquaporin water channels
331 (**Supplementary Table 5**), consistent with this mature endodermis cell type modulating
332 water permeability via aquaporins as well as through suberization.[32] We also identified
333 putative regulators of these stages by looking for transcription factors among the
334 genes that showed specificity for each endodermis cluster. The early endodermis type
335 showed a single upregulated transcription factor, ERF54, while the intermediate
336 subtype showed 14 upregulated transcription factors, including *KNAT7*, *SOMNUS*, and
337 *HAT22*. *MYB36*, which was found expressed in the late endodermis type, activates
338 genes involved in Casparian strip formation and regulates a crucial transition toward
339 differentiation in the endodermis.[33]
340
341 Overall, the combined information gained from transcriptional signatures of
342 developmental progression and endoreduplication highlights the importance of
343 integrating both open chromatin and transcriptional profiling to identify cell types or
344 cell states that may have otherwise been obscured in a single data type.

345
346 **Predicting regulatory events using integrated scRNA and scATAC data**
347
348 We previously identified transcription factor binding motifs that were enriched at
349 cell type-specific peaks in the root (**Figure 1D**). While individual motifs may be
350 associated with binding and activation by transcription factors, a sequence-level
351 analysis cannot distinguish among the many members of plant transcription factor
352 families that share near-identical sequence preferences. For example, WRKY family
353 motifs were highly enriched among epidermis and cortex accessible sites, but this
354 family contains >50 individual genes. In order to narrow down this list of genes to a few
355 possible candidates, we leveraged our nearest-neighbor annotation approach (**Figure**
356 **S2C**) to examine expression levels of all WRKY family transcription factors in the
357 scATAC data (**Figure 4A**). Overall, we found that the majority of WRKY members
358 showed expression in the epidermis, cortex or epidermal precursor cells (**Figure 4A**),
359 though some members showed stele-specific expression. To identify the most likely
360 members to bind the abundance of motifs in epidermis-specific peaks, we ranked
361 these genes by their specificity in the epidermis. The top four most specific genes,
362 *WRKY75*, *WRKY9*, *WRK6*, and *TTG2,* have documented roles in root development.[28,34–
363 36] *TTG2* shows strong specificity for the epidermis, but we also predict expression in
364 some cortex and precursor cells (**Figure 4B**). Two key interacting factors of *TTG2* that
365 also contribute to epidermis development, *GL2* and *TTG1*,[37,38] showed epidermis
366 expression and had correlated (Pearson correlation with *TTG2* across cells for *GL2* =
367 0.91, and *TTG1* = 0.47) patterns across all cells (**Figure S6B, S6C**).
368
369 Given the important role of *TTG2* in specification of atrichoblast fate in the
370 epidermis, we examined the consequences of its expression on accessibility of
371 individual peaks. Inference of individual regulatory events, particularly those involving
372 transcription factors, has long been a goal of studies that profile accessibility at
373 regulatory sites in bulk tissue. The varied cell states revealed by single-cell profiling
374 data, even those within a cell type, allow higher-resolution inference of these events.
375 To identify accessible sites that showed altered accessibility as a function of
376 transcription factor expression, we used a linear regression approach. We identified
377 617 peaks that showed significant (q-value < 0.05) associations with *TTG2* expression
378 levels (**Supplementary Table 6**). To visualize these associations using scATAC data,
379 we pseudobulked epidermis, cortex, and c/e precursor cells into four equal-sized bins
380 based on their level of *TTG2* expression (**Figure 4C**). Most significant associations
381 were positive, such that increased *TTG2* expression led to increased peak accessibility
382 (**Figure 4C**, top and lower-left panels), though negative associations could also be
383 identified (**Figure 4C**, lower-right panel). Positive associations occurred whether or not
384 a WRKY binding motif was present in the associated peak (**Figure 4C**), suggesting that
385 the role of WRKY transcription factors in specification of the epidermis likely requires
386 both direct and indirect regulatory events. Of peaks with significant (q-value < 0.05)
387 positive associations with *TTG2* expression, 80% of these contained a WRKY binding

motif, while only 38% of the peaks with negative associations contained a binding motif (**Figure 4D**). Overall, this analysis identifies transcription factors and putative target sites that constitute regulatory events important for specifying cell types; these genes and regulatory sites are good candidates for further functional studies.

Discussion

By profiling chromatin accessibility in the *A. thaliana* root at single-cell resolution, we assessed cell types, developmental stages, the transcription factors likely driving these stages and DNA copy number changes. We assigned over 5,000 root cells to tissues and cell types, demonstrating that these assignments are concordant with single-cell transcriptomic studies. These results answer an unresolved question in plant gene regulation: does the paucity of dynamic open chromatin sites seen in bulk profiling experiments represent an accurate reflection of uniform gene regulation in *A. thaliana* or does it reflect a confounding effect of bulk studies? We found that distinct root cell types show unique patterns of open chromatin sites, with approximately 1/3 of all accessible sites showing cell type-specific patterns. This estimate greatly exceeds the earlier estimates from bulk studies of only 5-10% of accessible sites showing tissue- or condition-specificity,[9] presumably due in part to tissue heterogeneity.

Although this single-cell ATAC study discovered many more dynamic accessible sites, the correlation between dynamic accessibility and gene expression in single cells remained poor, reminiscent of the equally poor correlation seen in bulk studies. We argue that the poor correlation between chromatin accessibility and gene expression is not a function of data quality. Instead, we propose that this weak correlation reflects the complex nature of regulatory processes underlying development. Although the correlation of chromatin accessibility and gene expression is weak at the level of individual loci, either the entirety of a cell's regulatory landscape or its transcriptome can independently capture its cell identity. It is this feature that allows joint co-embedding of both data types and the use of scRNA-seq data to annotate scATAC cells.

Thus, while the patterns of both chromatin accessibility and gene expression contain information on cell identity and development, the relationships between these patterns are not well-ordered or parsimonious. For the many cells belonging to a distinct cell type, gene expression results from direct and indirect regulatory events involving tens or hundreds of transcription factors and chromatin remodelers that do not necessarily act in concert. For any individual locus, then, the expectation that average accessibility predicts average expression breaks down. Without a simple one-to-one model to explain regulatory output, we are left with significant heterogeneity within and between cell types, and a subset of convergent expression or accessibility patterns that define cell type specificity. Alternative explanations for the discrepancy in accessibility and expression include: (1) maintenance of cell identity requires that a

cell's accessibility and expression profile stably reflect the convergent pattern for that cell type only a fraction of the time; and/or (2) cells have multiple accessibility and expression patterns that are sufficient to maintain cell identity and together constitute the convergent patterns we observe. In both scenarios, the heterogeneity in cell type specification will be buffered by factors outside chromatin accessibility or gene expression, such as spatial location in tissue, metabolic determinants of cell function or developmental age.

We posit that scATAC-seq data combined with scRNA-seq data will ultimately resolve these alternatives by enabling mechanistic models of gene regulatory networks. scATAC-seq data alone are sufficient to identify the full set of accessible sites in the *Arabidopsis* genome, and examination of the transcription factor motifs within these sites can enable predictions of regulatory networks. However, many plant transcription factor families are large, some containing over fifty members that recognize near identical motifs. Thus, the accessibility data must be integrated with single-cell expression data that capture cell type-specific expression of transcription factors in order to narrow down the most probable transcription factors that are enacting individual regulatory events. Building high resolution models of key regulatory events will require the expression level of individual transcription factors in a cell type, the accessibility of individual peaks in this cell type and the presence of binding motifs corresponding to the relevant transcription factors. Theoretically, a comprehensive capture of cell states with both open chromatin and transcriptional profiling will allow the ordering of gene regulatory events and the larger scale ordering of regulatory programs that underlie development. The ability to take single-cell measurements over distinct developmental stages will also increase the sampling of key regulatory events. Ultimately, achieving the goal of building models of gene regulatory events underlying development will require ever larger datasets to fully capture the range of possible cell states.

In the future, single-cell studies of more complex plant tissues in crops and other species will necessitate larger numbers of profiled cells and higher numbers of cuts per cell. In this way, approaches that maximize the number of cells profiled at low cost, such as single-cell combinatorial indexing,[39] will be critical. Annotation in future studies will also present a substantial challenge if a rich literature and genomic analyses, including single-cell transcriptome profiles, are not available. Nevertheless, as shown in this proof-of-principle study of the well-characterized *A. thaliana* root, the knowledge gained should eventually allow us to manipulate gene expression and organismal phenotype in a targeted manner.

Methods

Plant Material

475 *Genotype*: *Arabidopsis thaliana* ecotype Col-0 INTACT line *UBQ10*:NTF::*ACT2*:BirA
476 (available from ABRC, stock CS68649). *Growth conditions*: LD (16h light/8h dark), 22C,
477 ~100 µmol m2s, 50% RH. *Sample*: whole roots, harvested 12 days after germination,
478 from seedlings grown vertically on MS + 1% sucrose, atop filter paper (to facilitate root
479 harvesting).
480
481 *Nuclei Isolation and snATAC-seq*
482 Nuclei were isolated following a modified version of the protocol described in Giuliano
483 *et al*., 1988, as follows: 1g of roots was split in two batches of 0.5g, and each batch
484 chopped with a razor blade in 1 ml of Buffer A (0.8M sucrose, 10mM MgCl2, 25mM
485 Tris-HCl pH 8.0 and 1x Protease Inhibitor Tablet).[40] Extracts were combined, final
486 volume increased to 5ml with Buffer A, and incubated on ice for 10min, with gentle
487 swirling. The combined extract was filtered through miracloth, passed through a 26ga
488 syringe five times and re-filtered through a 40um cell strainer (BD Falcon). After
489 centrifugation at 2,000g 5min, the pellet was resuspended in 1ml Buffer B (0.4M
490 sucrose, 10mM MgCl2, 25mM Tris-HCl pH 8.0, 1x Protease Inhibitor Tablet, 1% Triton
491 X - 100) and loaded atop a 2-step 25/75 Percoll gradient (1 volume 25% Percoll in
492 Buffer B over 1 volume 75% Percoll in Buffer B). After centrifugation at 2,500g for
493 15min, nuclei were collected either at the 25/75 interface or in the subjacent 75
494 fraction, washed with 5 vols of Buffer B and recovered by centrifugation at
495 1,700g 5min. The nuclei pellet was resuspended in 100ul Buffer B + 1% BSA and any
496 nuclei clumps broken down by pipetting up and down multiple times. Nuclei yield with
497 this protocol was ~ 94,000 nuclei per gram of roots (fresh weight).
498 snATAC-seq libraries were built using the 10x Genomics Chromium Single Cell ATAC
499 Solution platform, following manufacturer's recommendations. Before transposition,
500 nuclei were spun 5min at 1,500g and resuspended in 10x Genomics Diluted Nuclei
501 Buffer, at a concentration of 3,200 nuclei/ul. 5ul of nuclei suspension were used for
502 transposition (16,000 nuclei being the maximum input recommended for 10x
503 Chromium, and 10,000 nuclei being the expected recovery).
504 *Combining and processing of root scRNA-seq data*
505 Samples were processed using the CellRanger vX.X pipeline from 10X Genomics,
506 including updated filtering of "halflet" cells that emerge due to multiply-barcoded
507 droplets.
508
509 *Integration of scRNA and scATAC data*
510 The R package Seurat version 3.1.5 was used to align and co-embed the scATAC-seq
511 data with scRNA-seq data published by Ryu et al. 2019, and to transfer cell type labels
512 from the scRNA data to the scATAC data.[30,41]
513
514 The standard workflow and default parameters as described in the Seurat vignette
515 "PBMC scATAC-seq Vignette" (satijalab.org/seurat/v3.1/atacseq_integration_vignette)
516 were used with the exception that all features (genes) were used when identifying
517 transfer anchors and performing the co-embedding rather than a set of "variable"
518 features as used in the vignette. Briefly this workflow is as follows:

An anchor set was established with the function FindTransferAnchors() linking the two datasets . Cell type annotations were transferred from the scRNA-seq data to the scATAC data using the function TransferData(). Pseudo RNA-seq count data was generated for the scATAC cells, again using the TransferData() function. The pseudo RNA data was then merged with the true scRNA-seq dataset and embedded in 2D UMAP space using Seurat functions.

A co-embedding was performed with a super-set of scRNA-seq data published by Jean-Baptiste et al. 2019, Shulse et al. 2019, Ryu et al. 2019. In the co-embedded space the scATAC-seq were found to be most closely co-located with data from Ryu2019. Based on this observation co-embedding was performed with the Ryu2019 dataset on its own.

Nearest neighbor analysis for transcriptional characterization of cells identified in scATAC assay

To annotate cells from the scATAC-seq assay with transcriptional features, we used average feature values from the nearest RNA neighbors in our co-embedded data (**Figure 2A**). In short, the 'distances' package in R was used to extract cell labels for the 25 nearest neighbors of each scATAC cell. For a feature of interest (individual gene expression, cell-cycle signature score, endoreduplication signature score, developmental progression signature), we calculated the mean expression from the 25 scRNA cells, and assigned that mean score to each ATAC cell (**Figure S2C**).

Motif analysis

Position weight matrices from the comprehensive DAP-seq dataset[27] were used as input into FIMO[42] to search for significant matches for each motif (adjusted p-value threshold < 1e-5) in each of the scATAC peaks. With the output of this motif scan, we generated a matrix that tallied counts of each motif within each peak. To identify motifs whose counts were significantly associated with cell type-specific accessibility, we first generated, for each peak, a relative accessibility score by taking the mean accessibility of that peak in each cell cluster relative to the overall accessibility of that peak in all clusters. Next, we used a linear regression framework within Monocle3[43] to identify individual motifs whose counts showed strong positive or negative correlations with the cell type-specific accessibility score in each cell cluster. The effect size of each motif's contribution to cell type-specific accessibility is given as the β of the linear regression, shown as a mean across all transcription factors in the same family.

Data Availability

Source data for all figures are available via Dryad (accession number pending). Expression data are available at the Gene Expression Omnibus (GEO number: pending).

Acknowledgements

We thank Dr. Ken Jean-Baptiste and Dr. Kerry Bubb for valuable discussions on ATAC-seq analysis. We also thank Xavi Guitart for helpful discussions on endoreduplication. This work was supported by the National Science Foundation (RESEARCH-PGR grant 17488843) to S.F. and C.Q. This work was also supported by NIH grant 1RM1HG010461 to C.Q. and S.F.

References

1. Brady, S. M. *et al.* A High-Resolution Root Spatiotemporal Map Reveals Dominant Expression Patterns. *Science (80-.).* **318**, 801–806 (2007).
2. Jean-Baptiste, K. *et al.* Dynamics of gene expression in single root cells of A. thaliana. *Plant Cell* **31**, tpc.00785.2018 (2019).
3. Shulse, C. N. *et al.* High-Throughput Single-Cell Transcriptome Profiling of Plant Cell Types. *Cell Rep.* **27**, 2241-2247.e4 (2019).
4. Zhang, T. Q., Xu, Z. G., Shang, G. D. & Wang, J. W. A Single-Cell RNA Sequencing Profiles the Developmental Landscape of Arabidopsis Root. *Mol. Plant* **12**, 648–660 (2019).
5. Ryu, K. H., Huang, L., Kang, H. M. & Schiefelbein, J. Single-cell RNA sequencing resolves molecular relationships among individual plant cells. *Plant Physiol.* **179**, 1444–1456 (2019).
6. Denyer, T. *et al.* Spatiotemporal Developmental Trajectories in the Arabidopsis Root Revealed Using High-Throughput Single-Cell RNA Sequencing. *Dev. Cell* **48**, 840-852.e5 (2019).
7. Sullivan, A. M. *et al.* Mapping and Dynamics of Regulatory DNA in Maturing Arabidopsis thaliana Siliques. *Front. Plant Sci.* **10**, 1–16 (2019).
8. Alexandre, C. M. *et al.* Complex relationships between chromatin accessibility, sequence divergence, and gene expression in arabidopsis thaliana. *Mol. Biol. Evol.* **35**, 837–854 (2018).
9. Sullivan, A. M., Bubb, K. L., Sandstrom, R., Stamatoyannopoulos, J. A. & Queitsch, C. DNase I hypersensitivity mapping, genomic footprinting, and transcription factor networks in plants. *Curr. Plant Biol.* **3–4**, 40–47 (2015).
10. Reynoso, M. A. *et al.* Evolutionary flexibility in flooding response circuitry in angiosperms. *Science (80-.).* **365**, 1291–1295 (2019).
11. Maher, K. A. *et al.* Profiling of accessible chromatin regions across multiple plant species and cell types reveals common gene regulatory principles and new control modules. *Plant Cell* **30**, 15–36 (2018).
12. Saunders, L. M. *et al.* Thyroid hormone regulates distinct paths to maturation in

pigment cell lineages. *Elife* **8**, (2019).
13. Gulati, G. S. *et al.* Single-cell transcriptional diversity is a hallmark of developmental potential. *Science (80-.).* **367**, 405–411 (2020).
14. Waddington, C. H. The Strategy of the Genes. (1959).
15. Orr-Weaver, T. L. When bigger is better: The role of polyploidy in organogenesis. *Trends Genet.* **31**, 307–315 (2015).
16. Derks, W. & Bergmann, O. Polyploidy in cardiomyocytes: Roadblock to heart regeneration? *Circ. Res.* **126**, 552–565 (2020).
17. Lang, L. & Schnittger, A. Endoreplication — a means to an end in cell growth and stress response. *Curr. Opin. Plant Biol.* **54**, 85–92 (2020).
18. Pirrello, J. *et al.* Transcriptome profiling of sorted endoreduplicated nuclei from tomato fruits: how the global shift in expression ascribed to DNA ploidy influences RNA-Seq data normalization and interpretation. *Plant J.* **93**, 387–398 (2018).
19. Bhosale, R. *et al.* A spatiotemporal dna endoploidy map of the arabidopsis root reveals roles for the endocycle in root development and stress adaptation. *Plant Cell* **30**, 2330–2351 (2018).
20. Robinson, D. O. *et al.* Ploidy and Size at Multiple Scales in the Arabidopsis Sepal. *Plant Cell* **30**, 2308–2329 (2018).
21. Blondel, V. D., Guillaume, J.-L., Lambiotte, R. & Lefebvre, E. Fast unfolding of communities in large networks. *J. Stat. Mech. Theory Exp.* **10**, P10008 (2008).
22. Shu, H., Wildhaber, T., Siretskiy, A., Gruissem, W. & Hennig, L. Distinct modes of DNA accessibility in plant chromatin. *Nat. Commun.* **3**, (2012).
23. Sullivan, A. M. *et al.* Mapping and dynamics of regulatory DNA and transcription factor networks in A. thaliana. *Cell Rep.* **8**, 2015–2030 (2014).
24. McFaline-Figueroa, J. L., Trapnell, C. & Cuperus, J. T. The promise of single-cell genomics in plants. *Curr. Opin. Plant Biol.* **54**, 114–121 (2020).
25. Cao, J. *et al.* Joint profiling of chromatin accessibility and gene expression in thousands of single cells. *Science (80-.).* **1385**, 1380–1385 (2018).
26. Spitz, F. & Furlong, E. E. M. Transcription factors: From enhancer binding to developmental control. *Nat. Rev. Genet.* **13**, 613–626 (2012).
27. O'Malley, R. C. *et al.* Cistrome and Epicistrome Features Shape the Regulatory DNA Landscape. *Cell* **165**, 1280–1292 (2016).
28. Johnson, Cameron S.; Kolevski Ben, and S. D. R. TRANSPARENT TESTA GLABRA2 , a Trichome and Seed Coat Development Gene of Arabidopsis, Encodes a WRKY Transcription Factor. *Plant Cell* **14**, 1359–1375 (2017).
29. Stuart, T. *et al.* Comprehensive Integration of Single-Cell Data. *Cell* **177**, 1888-1902.e21 (2019).
30. Butler, A., Hoffman, P., Smibert, P., Papalexi, E. & Satija, R. Integrating single-cell transcriptomic data across different conditions, technologies, and species. *Nat. Biotechnol.* **36**, 411–420 (2018).
31. Gulati, G. S. *et al.* Single-cell transcriptional diversity is a hallmark of developmental potential. *Science (80-.).* **367**, 405–411 (2020).

32. Kreszies, T., Schreiber, L. & Ranathunge, K. Suberized transport barriers in Arabidopsis, barley and rice roots: From the model plant to crop species. *J. Plant Physiol.* **227**, 75–83 (2018).
33. Liberman, L. M., Sparks, E. E., Moreno-Risueno, M. A., Petricka, J. J. & Benfey, P. N. MYB36 regulates the transition from proliferation to differentiation in the Arabidopsis root. *Proc. Natl. Acad. Sci. U. S. A.* **112**, 12099–12104 (2015).
34. Devaiah, B. N., Karthikeyan, A. S. & Raghothama, K. G. WRKY75 transcription factor is a modulator of phosphate acquisition and root development in Arabidopsis. *Plant Physiol.* **143**, 1789–1801 (2007).
35. Chen, Y. F. *et al.* The WRKY6 transcription factor modulates PHOSPHATE1 expression in response to low pi stress in arabidopsis. *Plant Cell* **21**, 3554–3566 (2009).
36. Zheng, X. *et al.* MdWRKY9 overexpression confers intensive dwarfing in the M26 rootstock of apple by directly inhibiting brassinosteroid synthetase MdDWF4 expression. *New Phytol.* **217**, 1086–1098 (2018).
37. Long, Y. & Schiefelbein, J. Novel TTG1 Mutants Modify Root-Hair Pattern Formation in Arabidopsis. *Front. Plant Sci.* **11**, 1–12 (2020).
38. Schiefelbein, J., Kwak, S. H., Wieckowski, Y., Barron, C. & Bruex, A. The gene regulatory network for root epidermal cell-type pattern formation in arabidopsis. *J. Exp. Bot.* **60**, 1515–1521 (2009).
39. Cao, J. *et al.* Comprehensive single-cell transcriptional profiling of a multicellular organism. *Science (80-.).* **357**, 661–667 (2017).
40. Giuliano, G. *et al.* An evolutionarily conserved protein binding sequence upstream of a plant light-regulated gene. *Proc. Natl. Acad. Sci. U. S. A.* **85**, 7089–7093 (1988).
41. Stuart, T. *et al.* Comprehensive Integration of Single-Cell Data Resource Comprehensive Integration of Single-Cell Data. *Cell* **177**, 1888-1902.e21 (2019).
42. Grant, C. E., Bailey, T. L. & Noble, W. S. FIMO: Scanning for occurrences of a given motif. *Bioinformatics* **27**, 1017–1018 (2011).
43. Cao, J. *et al.* The single-cell transcriptional landscape of mammalian organogenesis. *Nature* **566**, 496–502 (2019).

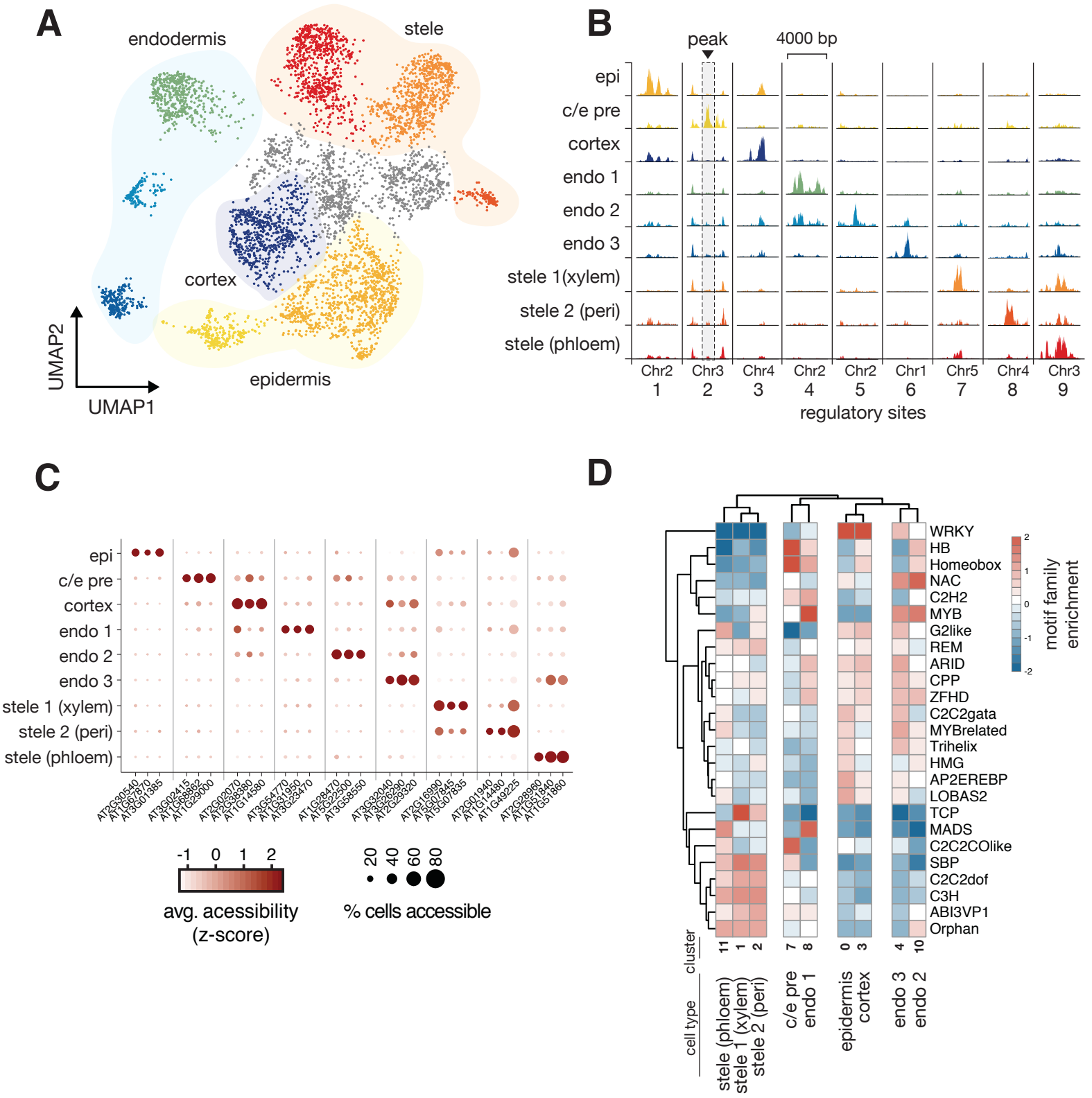

Figure 1. scATAC-seq identifies known root cell types.

Figure 1. scATAC-seq identifies known root cell types. (A) UMAP dimensionality reduction plot of root cells using peak-level scATAC data. Cells are colored according to Louvain clusters, and broad tissue types are indicated with transparent blobs. (B) Pseudo-bulked peak tracks generated by combining ATAC data from all cells within a cluster. Each column represents a single locus in the genome that shows cell type-specific accessibility; one example is shown for each cell type. Colors match those in previous panel. (C) Dotplot showing marker genes for each cell type cluster. Each column represents a single gene's activity score, the summed accessibility of its gene body and promoter sequence (-400bp from transcription start site). The color of each point indicates the magnitude of accessibility and the size of each point represents the fraction of cells in each type showing accessibility at that gene. (D) Heatmap showing the predicted effect, across all peaks, of motifs from each *Arabidopsis* transcription factor family on cell type specific accessibility. Darker shades of red indicate that presence of the motif is correlated with increased accessibility in that cell type, while shades of blue indicate that the motif is anti-correlated with accessibility. The mean effect all transcription factors within a given family are shown as rows, and each column represents a cell type.

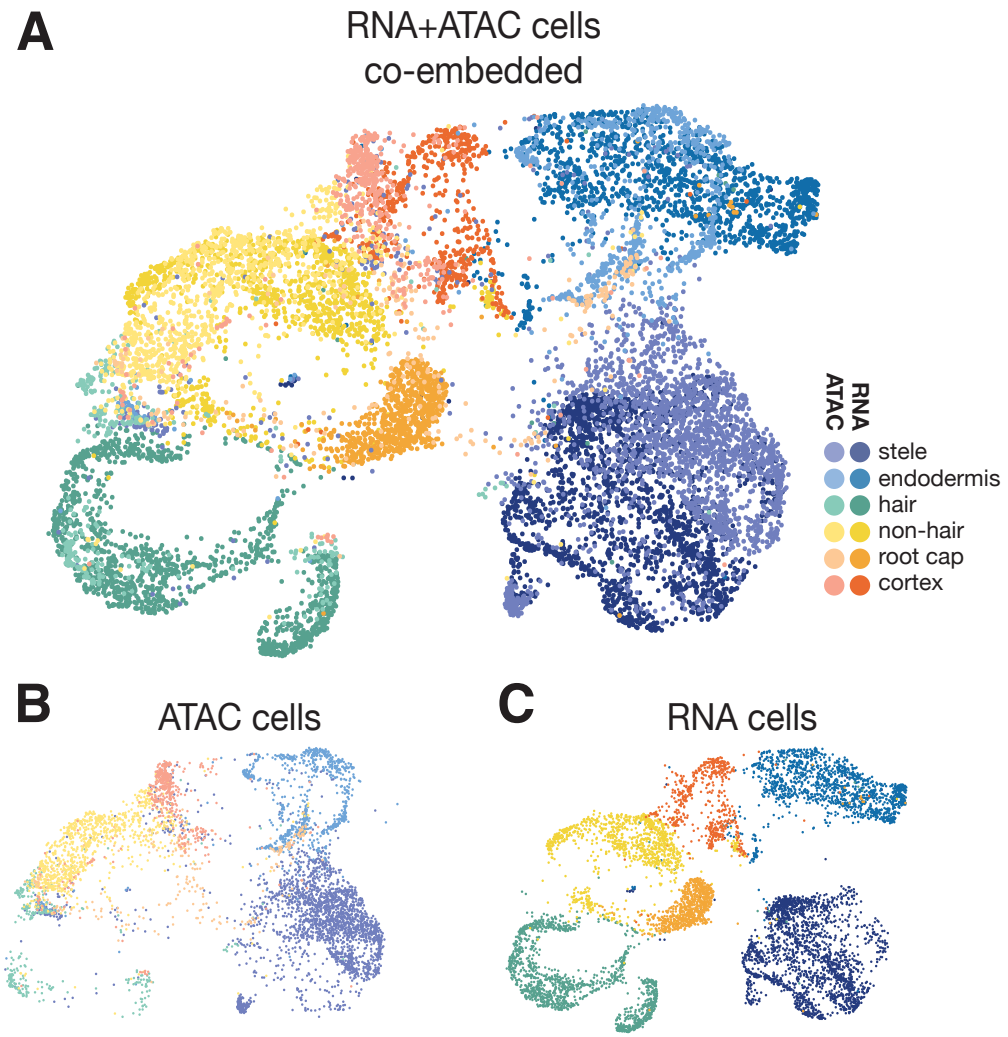

Figure 2. scATAC-seq data can be integrated with scRNA-seq data to identify cell types.

Figure 2. scATAC-seq data can be integrated with scRNA-seq data to identify cell types. (A) UMAP co-embedding of root scATAC cells alongside root scRNA cells (Schief et al). Cells are colored by broad tissue type, with scATAC cells colored in lighter shades and scRNA cells in darker shades. (B) UMAP from (A), but showing only cells from the scATAC-seq experiment; (C) shows only cells from the scRNA-seq experiment.

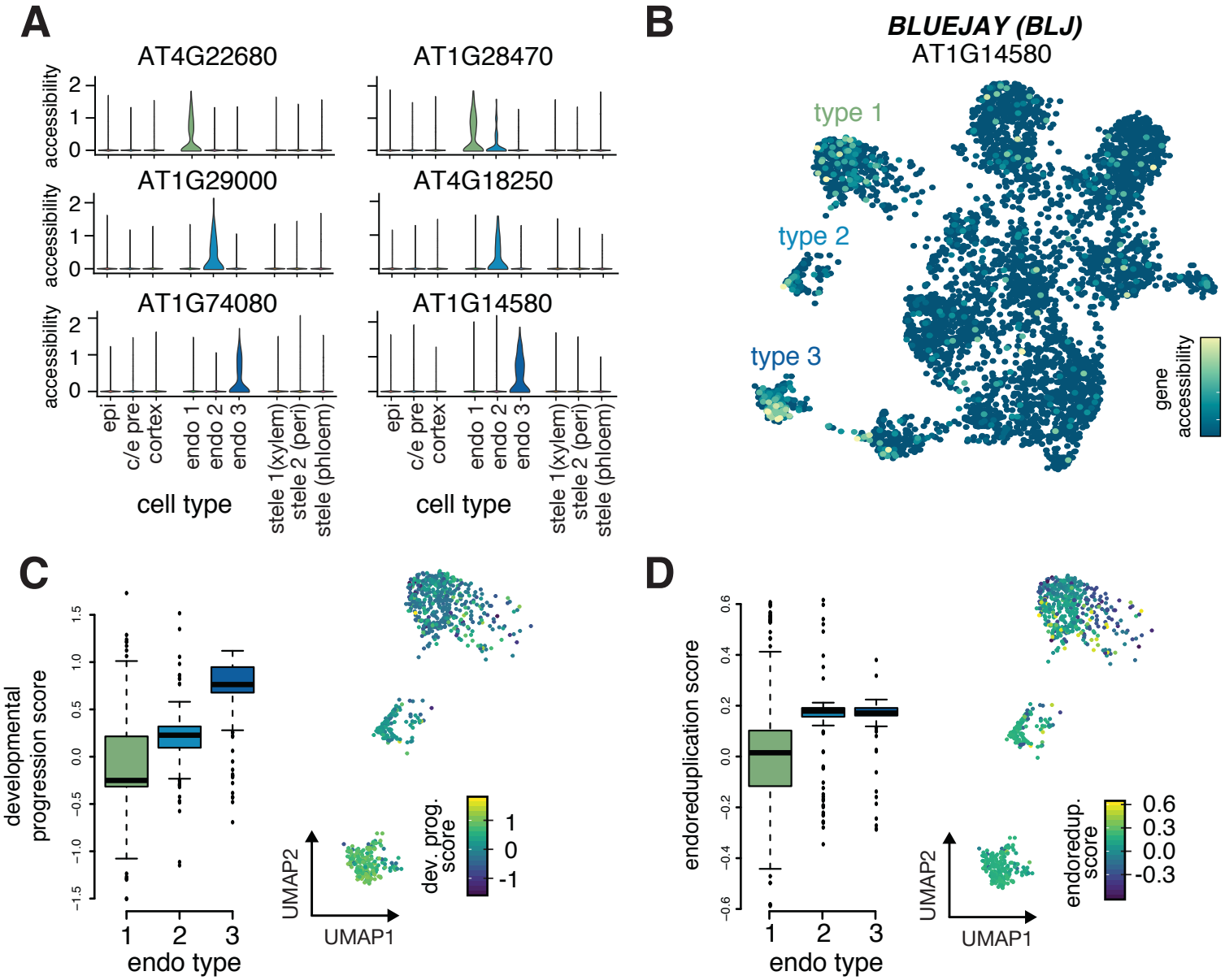

Figure 3. scATAC-seq identifies distinct sub-types of endodermal cells.

Figure 3. scATAC-seq identifies distinct sub-types of endodermal cells. (A) Violin plots showing specific patterns of accessible genes that mark each endodermal type. Two examples are given for each endodermal type, and gene-level accessibility scores are shown additionally for all other cell types. (B) UMAP of all cells colored by accessibility of the *BLUEJAY* gene, which marks endodermal type 3; corresponding violin plot for this gene in lower right panel in (A). (C) Boxplot showing an increase in median developmental progression of each endodermal type, as determined by average transcriptional complexity in the nearest 25 scRNA neighbors of each scATAC cell in the co-embedded representation from Fig. 2A; right inset shows UMAP of endodermal cells with each cell colored by the average developmental progression of its scRNA neighbors, mirroring the gradual increase seen in left panel. (D) Boxplot showing an increase in median levels of endoreduplication across endodermal types, ascertained as in (C), but instead using a gene expression signature of endoreduplication; right inset shows UMAP of endodermal cells with each cell colored by the average endoreduplication score of its scRNA neighbors, with highest levels seen in endodermal types 2 and 3.

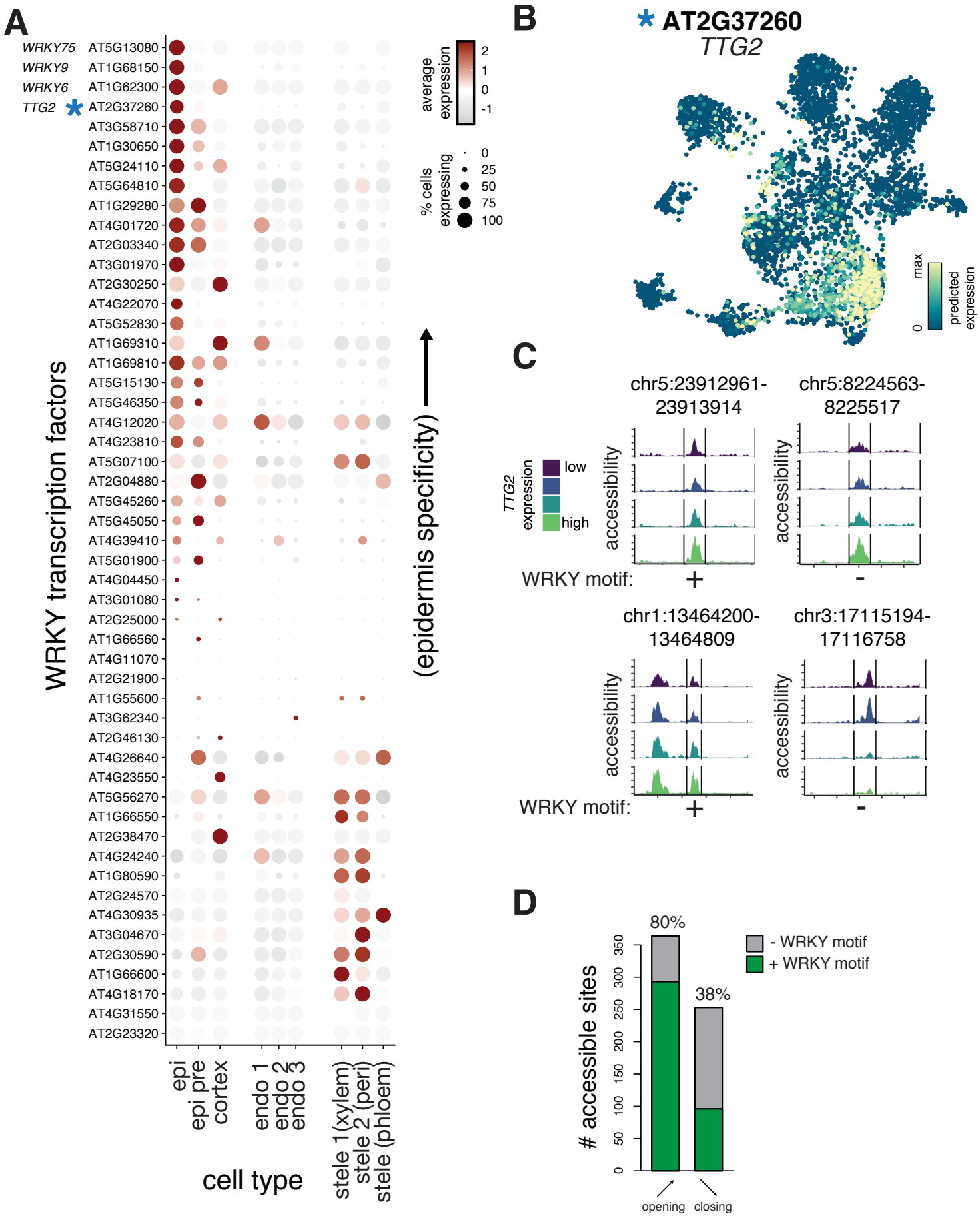

Figure 4. Integration of scATAC and scRNA-seq data allows prediction of candidate regulatory TFs and genes.

Figure 4. Prediction of candidate regulatory transcription factors from integrated scATAC and scRNA data. (A) Dotplot heatmap showing predicted expression of all WRKY family transcription factors across all cells; rows are ordered by the specificity of their epidermis expression. (B) UMAP plot of cells derived from scATAC experiment, but colored by predicted expression of an epidermis-specific WRKY transcription factor, *TTG2*. (C) Pseudobulked accessibility tracks of epidermis peaks whose accessibility shows a significant association with predicted *TTG2* expression. Cells with higher TTG2 expression are shown in lighter shades. All panels show examples of significant ($q < 0.05$) positive associations of *TTG2* expression with peak accessibility except the lower right panel. In each case, the presence of a WRKY binding motif is indicated below the peak. (D) Barplot showing fraction of WRKY binding motifs in peaks of the epidermis, cortex, and pre-cursor type that showed significant association with *TTG2* expression. Peaks whose accessibility showed positive associations with expression are labelled as "opening" and those with negative associations with expression are labeled as "closing."

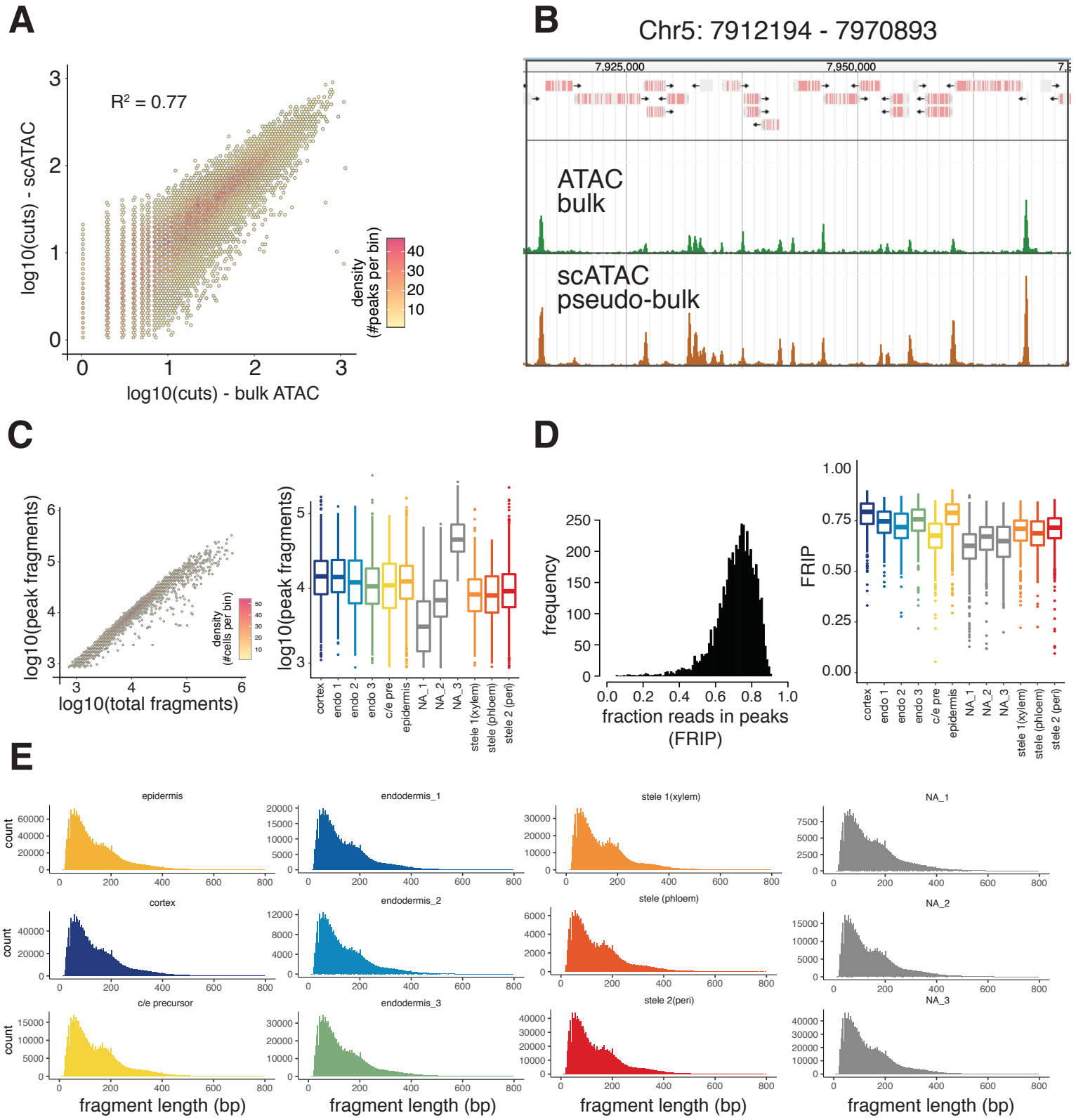

Supplementary Figure 1. Quality of scATAC-seq data is comparable to bulk ATAC-seq data.

Supplementary Figure 1. Quality of scATAC-seq data is comparable to bulk ATAC-seq data. (A) Scatterplot where each point represents peak defined in the scATAC data, and the x-axis shows the total cutcount within those peaks in bulk ATAC-seq and the y-axis shows the total cutcount within those peaks in scATAC-seq. Point density is indicated by increasing shades of red. (B) Example genomic region showing bulk ATAC accessibility (green) and pseudobulked scATAC accessibiltity (brown). Gene models are indicated above. (C) Read recovery per cell: Left panel shows relationship between total reads recovered per cell (x-axis) and reads in peaks (y-axis). Areas with higher point density are shown as in (A). Right panel shows boxplots of total number of reads in peaks recovered for each cell type. (D) ATAC quality per cell: Left panel shows overall distribution of fraction reads in peaks (FRIP) across all cells, right panel shows distribution of FRIP for each cell type. (E) Read length distributions for all fragments separated by cell type.

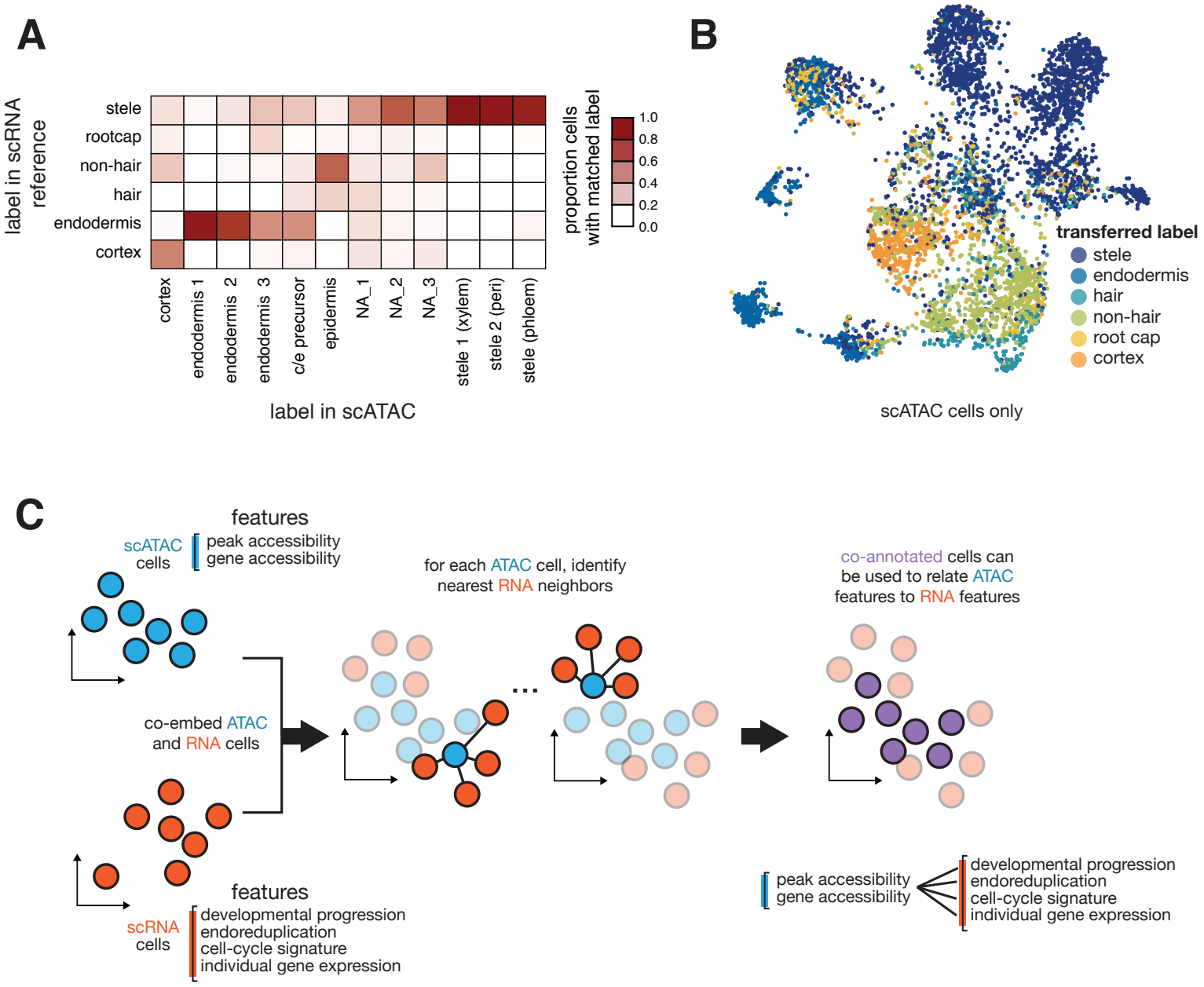

Supplementary Figure 2. Co-embedding-derived cell-type labels match manual annotations.

Supplementary Figure 2. Co-embedding of scATAC and scRNA data allows validation of cell type labels and annotation by RNA-derived features. (A) Confusion matrix showing the correspondence of manual cell annotations with those derived from the label-transfer from RNA to ATAC cells. (B) UMAP of scATAC cells as in Fig. 1A, but cells are colored by the cell type label predicted from annotations of scRNA nearest neighbors. These cell types labels broadly match those predicted by manual annotation, and separate the epidermis cluster into hair and non-hair cells. (C) Workflow schematic for annotation of scATAC-cells with transcriptional data. In short, the 25 nearest RNA neighbors from each ATAC cell in the co-embedded graph (**Figure 2A**) were identified, and average expression of individual genes and signatures scores were computed and assigned to each ATAC cell.

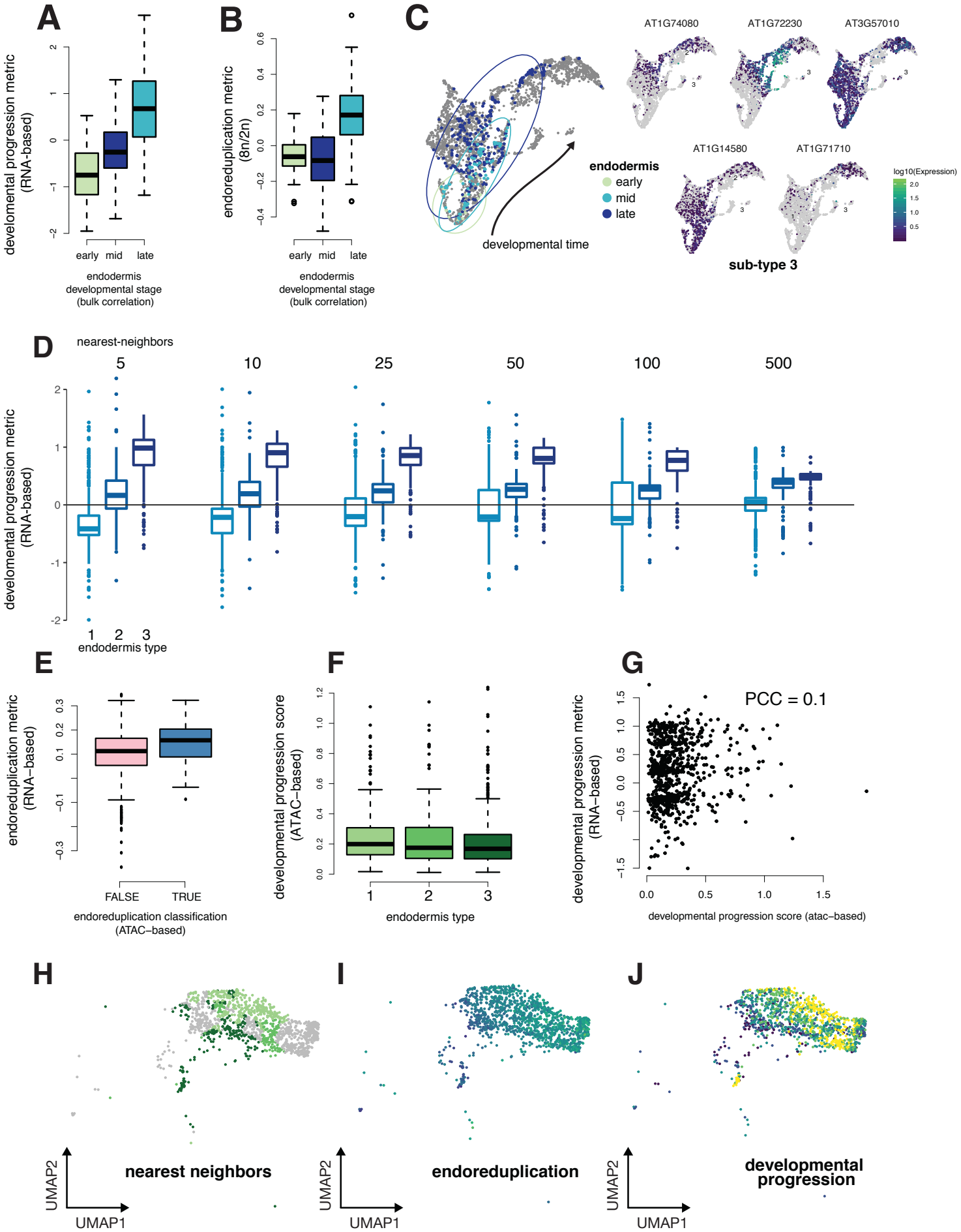

Supplementary Figure 3. scATAC-seq identifies distinct sub-types of endodermal cells.

Supplementary Figure 3. Characterization of endodermal sub-types with combined scATAC and scRNA-seq data. Boxplots showing that developmental progression scores (A) and endoreduplication scores (B) are consistent with a previously described annotations of developmental progression of the endodermis (Jean-Baptiste et al). Cells were grouped into early, middle and late (left to right) developmental stages by Jean-Baptiste et al. (C) UMAP of endodermal cells from multiple scRNA-seq studies, with developmental stage designations of cells from the Jean-Baptsite at al study highlighted. Inset shows variable expression patterns of genes with highly specific accessibility patterns in scATAC data. (D) Boxplots showing the transcriptional-signature-based endoreduplication metric compared to a binary classification of endoreduplication cells using scATAC data. scATAC cells with high levels of cutcounts at a single locus (suggesting endoreduplication) were analyzed in the co-embedded graph with scRNA-seq cells to calculate the average level of the endoreduplication signature among each scATAC cell's 25 nearest neighbors. The overall trend shows that the cutcount-based classification of endoreduplication is consistent with the transcriptional-signature-based metric. (E.) Boxplots showing levels of accessible genes (analogous to transcriptional complexity metric from Fig. 3C, only computed as total number of accessible genes rather than total number of transcribed genes). The overall trend remains the same, with progressive loss of complexity in the later endodermal types, but the ATAC-based metric shows less sensitivity than the RNA-based one. (F) Scatterplot showing poor correlation of ATAC-based developmental progression score and the RNA-based score. (G-I) Subset of co-embedded UMAP from Figure 2A showing only endodermal cells; nearest RNA neighbors for each endodermal type are shown in (G); (H) shows RNA cells colored by transcriptional-signature-based endoreduplication metric; (I) shows RNA cells colored by transcriptional complexity metric.

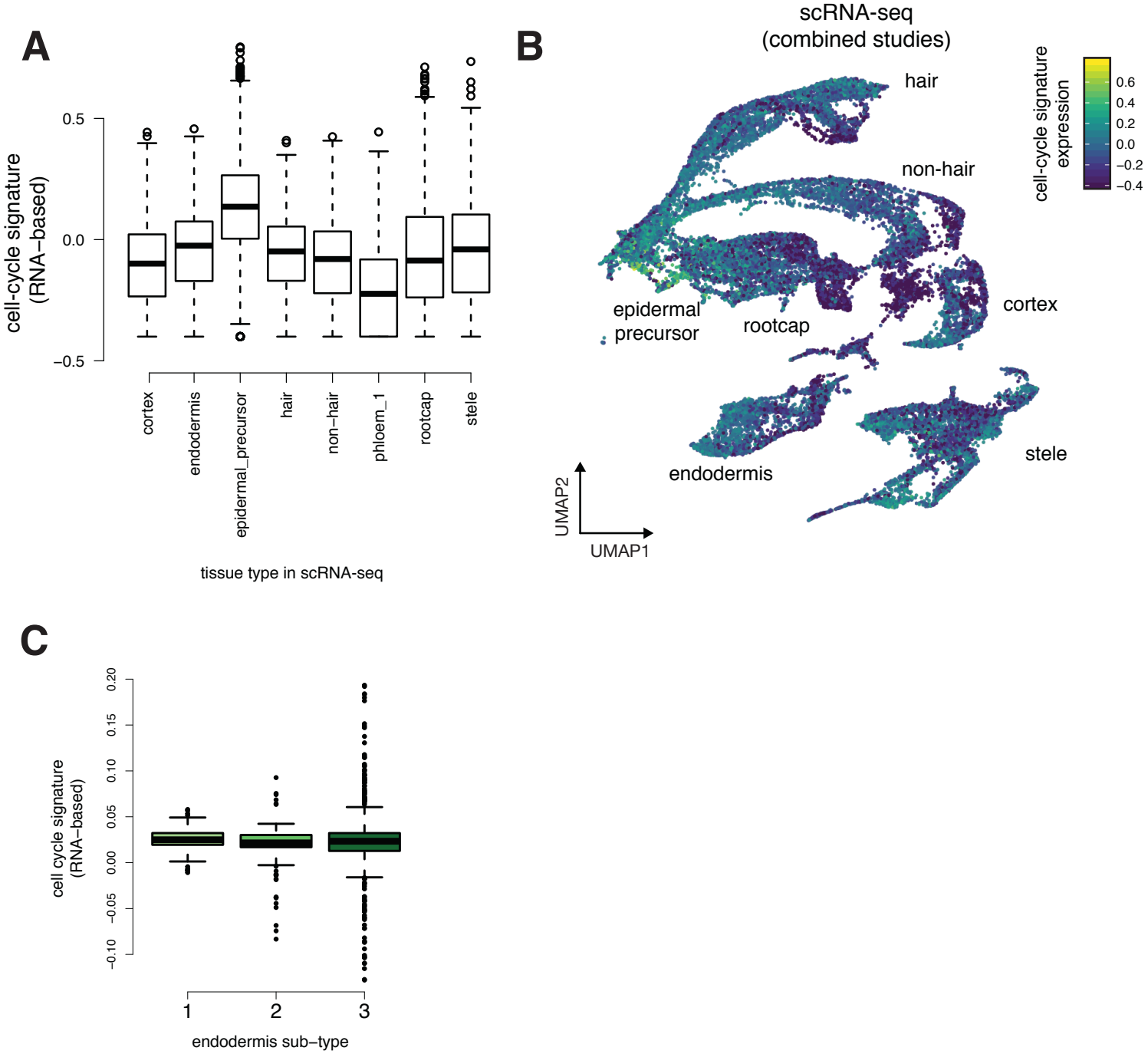

Supplementary Figure 4. Dividing cells are present in the root, but do not distinguish endodermis sub-types

Supplementary Figure 4. Dividing cells are present in the root, but are not a distinguishing feature of endodermal types. (A) Boxplots showing levels of a cell-cycle signature in each scRNA-seq root cell type. (B) UMAP plot of combined root scRNA-seq studies with each cell colored by its expression the cell cycle signature. (C) Cell cycle signature predicted from nearest neighbors of endodermis types (as in **Figure 3C, 3D**) shows that proliferation is not a strongly distinguishing feature between types.

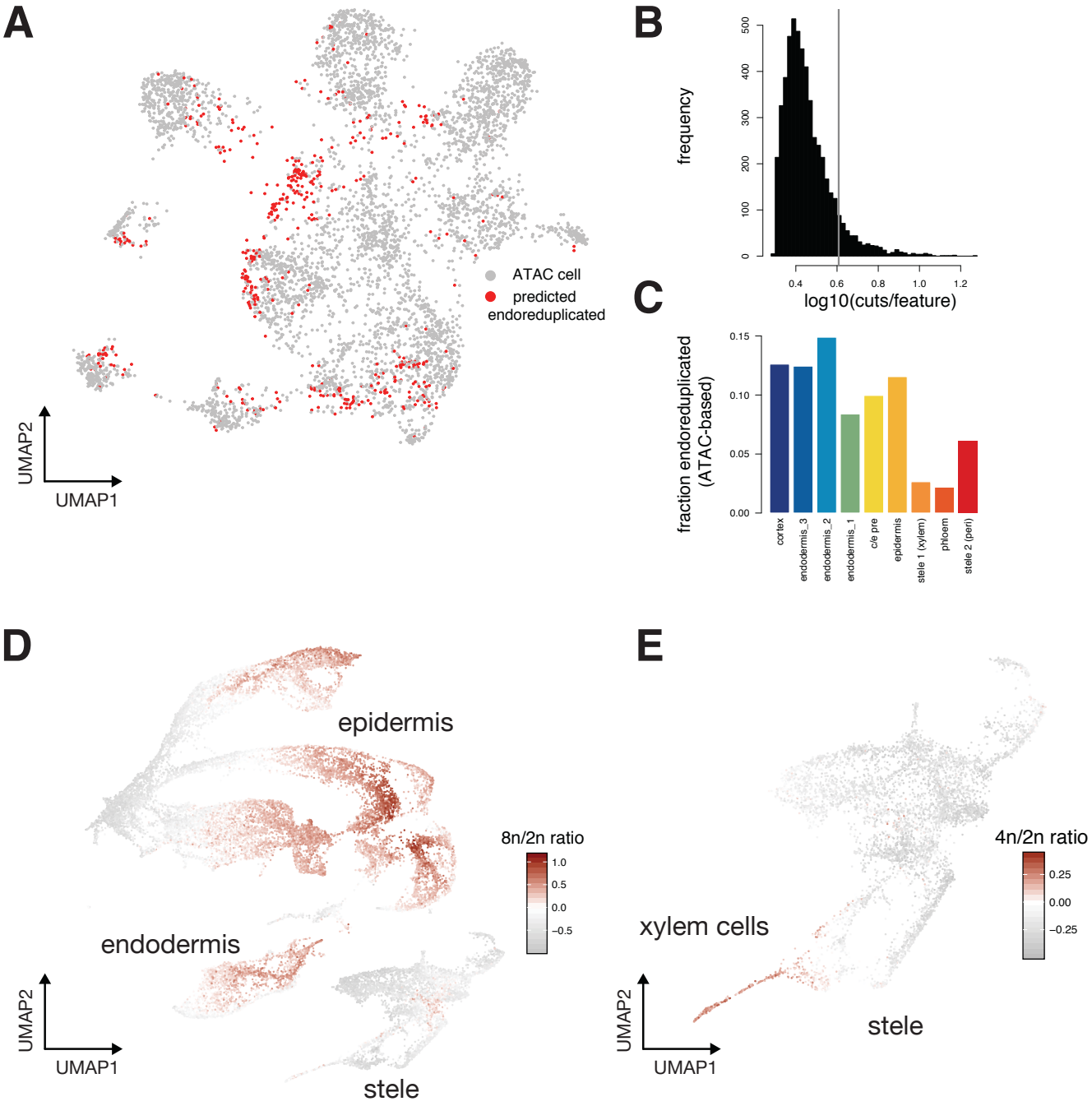

Supplementary Figure 5. Endoreduplicated cells can be identified in both scATAC and scRNA-seq data

Supplementary Figure 5. Approaches for identifying endoreduplicated cells in both scATAC and scRNA-seq data. (A) UMAP plot of root scATAC cells, each colored based on whether that cell contains a threshold level of cuts per site. (B) Histogram showing the log cuts per site across all cells, with the threshold used to color cells in (A) shown as a vertical grey line. (C) Barplot showing the fraction of cells in each type that show putative endoreduplication, as determined by the threshold cuts per site drawn in (B). In general, cell layers nearer the epidermis show higher fractions of endoreduplicated cells, while cell layers of the stele showed lower levels. (D) UMAP of root scRNA cells, each colored based on the expression level of a transcriptional signature for endoreduplication, as determined by a ratio of expression levels in genes previously determined as enriched in 8n cells over those enriched in 2n cells. (E) A known instance of endoreduplication in the stele is identified by a metric similar to (D), except that cells are colored by signature for 4n cells (ratio of 4n-specific genes to 2n-specific genes).

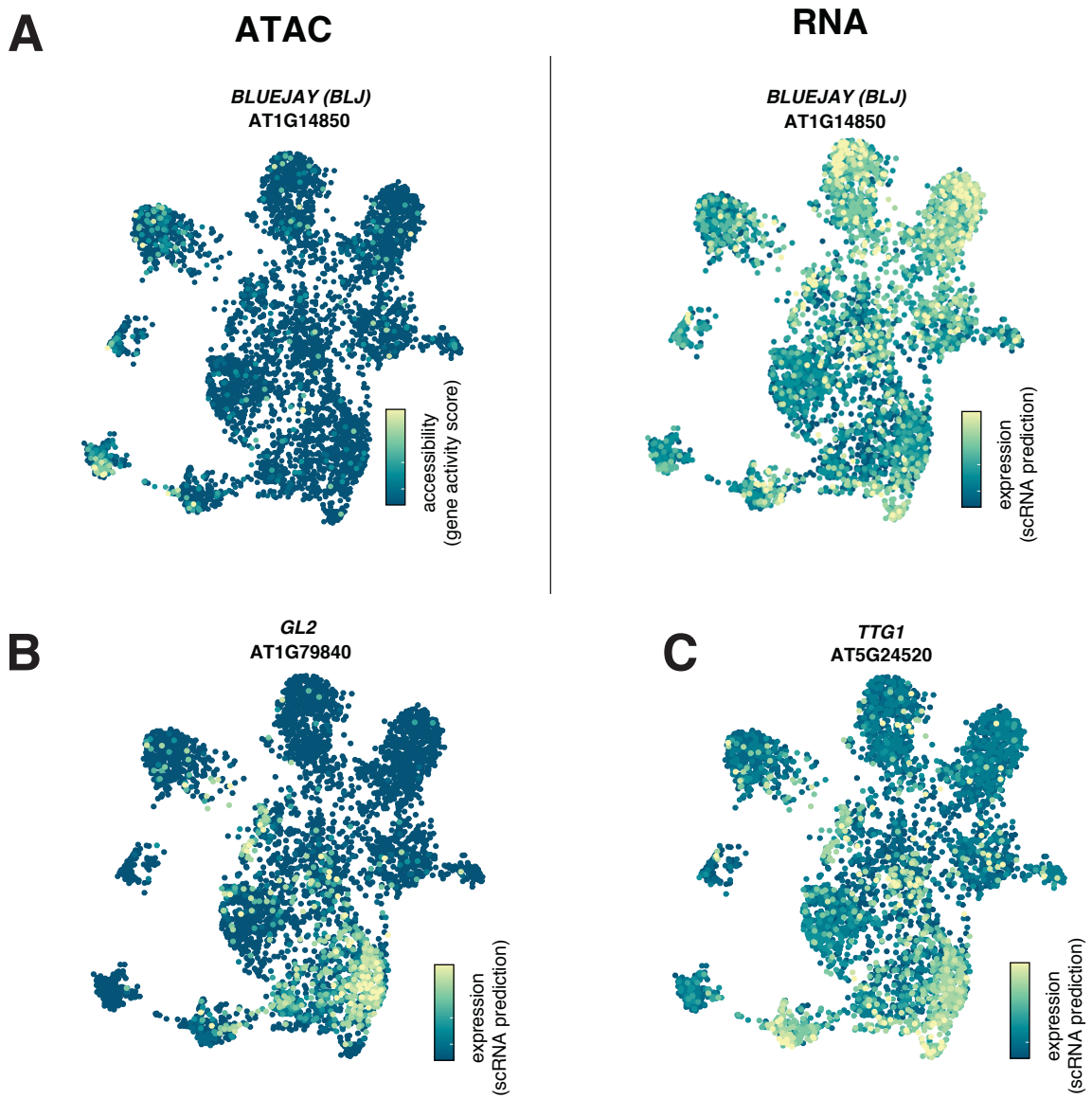

Supplementary Figure 6. Identifying transcription factors involved epidermal specification.

Supplementary Figure 6. Identifying transcription factors involved in tissue specification. (A) Left panel shows UMAP of scATAC cells colored by level of accessibility at the *BLUEJAY*, and right panel shows the same cells colored by predicted expression level of *BLUEJAY.* (B) UMAP of scATAC cells colored by predicted expression level of epidermal specification factor *GL2.* (C) UMAP of scATAC cells colored by predicted expression level of epidermal specification factor *TTG1*.